An Assessment of the Fe-O System

By B. Sundman
Division of Physical Metallurgy
Royal Institute of Technology
S-100 44 Stockholm, Sweden

The Fe-O system is well known experimentally and has a number of characteristic features in the liquid and solid phases—for example, extended solubility of the solid oxides, magnetic transitions, and a liquid miscibility gap. In this paper, these properties are described using the compound energy model with ionic constituents for the solid phases and an ionic two-sublattice model for the liquid. Parameters in these models are assessed to describe the experimental data, and a consistent set is determined that gives an accurate description of the properties from 298.15 to 2000 K.

Introduction

The Fe-O system provides a challenging opportunity for application of the new sophisticated technique usually known as the "Calphad method." This technique consists of modeling the thermodynamics of each phase using a mathematical expression and methods to assess a number of model parameters to fit the experimental data of the thermodynamics and phase diagram of a system. This assessment technique, in which many different types of information can be used simultaneously, makes it possible to obtain a consistent description that is more reliable than a set of parameters derived from each type of data separately. This assessment technique is also necessary to use data from lower order systems for extrapolations into multicomponent systems.

Selected Experimental Data

The available experimental data in the Fe-O system were reviewed recently by Spencer and Kubaschewski,[1] and in the present work, their select data were accepted in most cases. Most experimental works on this system are fairly consistent with each other.

Wüstite

In wüstite, the oxygen activity has been measured by several authors,[2-12] and agreement generally is good among different sources. The measurements of the solubility limits of wüstite were not used as primary data in the present assessment, except at the three invariant equilibria. The first, with bcc and magnetite, and the second, with fcc and liquid, were taken from the paper by Darken and Gurry,[3] and the third, with liquid and magnetite at 1697 K, from the second paper by Darken and Gurry.[13] Data for the oxygen activity in the two-phase region wüstite + Fe were taken from Sjödén *et al.*[14] and from Takayama and Kimizuka.[15] For the two-phase region wüstite + magnetite, oxygen activity data from Carel[16] and Barbero *et al.*[17] were used. Although wüstite decomposes around 830 K to magnetite and ferrite, it is possible to prevent this by rapid cooling. Thus, the low-temperature properties of wüstite have been measured, and the values for $S(298)$ and $\Delta_f H(298)$ were taken from the work by Todd and Bonnickson.[18] No data for the heat capacity were used, but enthalpy data were taken from Coughlin *et al.*[19]

Magnetite

The values for $S(298)$ and $\Delta_f H(298)$ for magnetite were taken from Grönvold and Sveen[20] and Roth and Bertram.[21] As the magnetite is a fully ordered inverse spinel at low temperature, a residual entropy contribution of $2R \ln 2$ at 0 K was included in the $S(298)$. Heat capacity data and enthalpy data from Coughlin *et al.*[19], Grönvold and Sveen[20], Westrum and Grönvold,[22] and Esser *et al.*[23] were used. A value for the Gibbs energy of formation of magnetite at 800 K from Barbi[24] was included.

Magnetite gradually changes from inverse to almost random order with increasing temperature. Measurements of this ordering and the oxygen activity in the single-phase region by Dieckmann[25] and Wu and Mason[26] were used.

Jacobson and Rosén[27] have measured the difference of the oxygen potential in the wüstite + magnetite and magnetite + hematite two-phase regions, and this information was included in the optimization, as well as measurements by Norton,[28] Dieckmann,[25] and Darken and Gurry[3] on the oxygen activity in the two-phase region magnetite + wüstite.

Hematite

For hematite, the data for $\Delta_f H(298)$ and S(298) were taken from Coughlin *et al.*,[19] who also have determined enthalpy differences at various temperatures. Heat capacity measurements were taken from Grönvold and Samuelson,[29] Krupka,[30] and Grönvold and Westrum.[31]

Liquid

The select data for the liquid phase were taken mainly from Darken and Gurry,[13] who have reported both oxygen activities and phase diagram information. Oxygen activities in the metallic liquid were taken from Tankins *et al.*,[32] Schwerdtfeger,[33] Gatellier and Olette,[34] and Dastur and Chipman.[35] Coughlin *et al.*[19] have measured the enthalpy differences among wüstite specimens up into the liquid range, and this information has been included. The solubility of oxygen in metallic liquid from Hepworth *et al.*[36] was used.

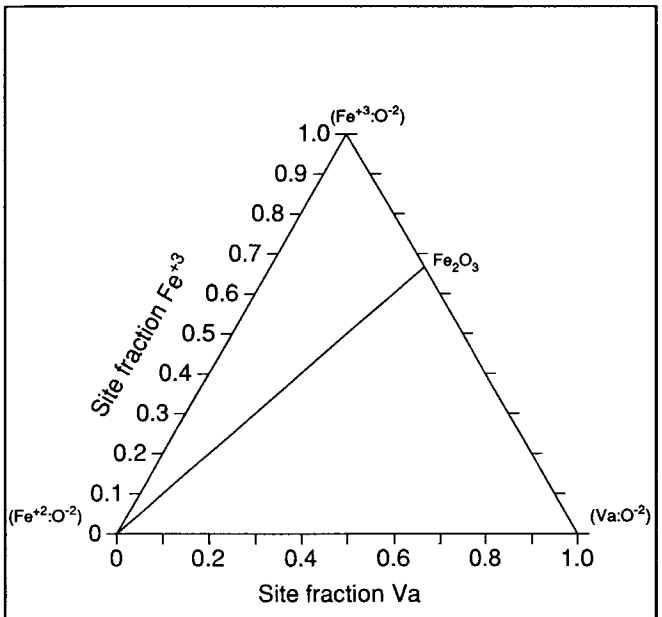

Fig. 1 Structural model of wüstite ($Fe_{0.947}O$). Two of the corners have a net charge and are thus unphysical. The line from the FeO corner to Fe_2O_3 represents possible neutral compositions.

fcc and bcc Phases

The solubilities of oxygen measured by Swisher and Turkdogan[37] were used to determine the thermodynamic properties of oxygen in the fcc and bcc phases of iron.

Models

In modeling the thermochemical properties of phases where an appreciable number of the sites may be vacant, it is convenient to use the formula unit of a phase as basis for expressing the Gibbs energy of the phase. It is easy to obtain the Gibbs energy per mole of real atoms by dividing with the total number of sites occupied with real atoms.

One must also select a reference state for the thermochemical data for the components, and in accordance with the SGTE[38] recommendations, we have used the stable state at 298.15 K and 1 bar as the reference state. This is denoted SER in the expression below.

The phases in the Fe-O system have characteristic names, but these phases have simple structures that appear also in other oxide and ionic systems. As the current work is a first step toward a general thermodynamic database for oxides and other phases, it is convenient to introduce generic phase names rather than those used in a particular system. For example, the phases wüstite, lime (CaO), and periclase (MgO) all have the same structure and can dissolve each other to a larger or lesser extent. Following a suggestion by Barry,[39] the generic name halite, from the NaCl system, was adopted for wüstite. For magnetite, the generic name is spinel, and for hematite, it is corundum.

fcc and bcc Phases

For the iron phases, the solubility of oxygen is very small. It does not matter which model is used to describe such small solubilities.

Table 1 Assessed Parameters for the Fe-O System

The magnetic contribution to Gibbs energy is described by:

$G^{mo}_{mix} = RT \ln(\beta + 1) f(\tau)$, $\tau = T/T_C$

For $\tau < 1$:

$$f(\tau) = 1 - \left[\frac{79\tau^{-1}}{140p} + \frac{474}{497}\left(\frac{1}{p} - 1\right)\left(\frac{\tau^3}{6} + \frac{\tau^9}{135} + \frac{\tau^{15}}{600}\right)\right]/A$$

and for $\tau > 1$:

$$f(\tau) = -\left(\frac{\tau^{-5}}{10} + \frac{\tau^{-15}}{315} + \frac{\tau^{-25}}{1500}\right)/A$$

where $A = \left(\frac{518}{1125}\right) + \left(\frac{11692}{15975}\right)\left[\left(\frac{1}{p}\right) - 1\right]$ and p depends on the structure.

In the superscripts below an H is used as prefix for some phase names in order to denote a hypothetical phase without a magnetic contribution.

Gas

$${}^0G^{GAS}_{O_2} - 2H^{SER}_O = +G(O_2,GAS)$$

Ionic-liquid

$${}^0G^{IONIC-LIQ}_{Fe^{+2}:O^{-2}} - H^{SER}_{Fe} - H^{SER}_O = +4G(FeO,liq)$$

$${}^0G^{IONIC-LIQ}_{Fe^{+3}:O^{-2}} - H^{SER}_{Fe} - H^{SER}_O = +5\,G(FeO,liq) - 180\,9555 + 80.574\,T$$

$${}^0G^{IONIC-LIQ}_{Fe^{+2}:Va} - H^{SER}_{Fe} = +G(Fe,liq)$$

$${}^0G^{IONIC-LIQ}_{Fe^{+3}:Va} - H^{SER}_{Fe} = +G(Fe,liq) + 200\,000$$

$${}^0L^{IONIC-LIQ}_{Fe^{+2},Fe^{+3}:O^{-2}} = 26\,362$$

$${}^1L^{IONIC-LIQ}_{Fe^{+2},Fe^{+3}:O^{-2}} = 13\,353$$

$${}^0L^{IONIC-LIQ}_{Fe^{+2}:O^{-2},Va} = +83\,502 + 34.784\,T$$

$${}^1L^{IONIC-LIQ}_{Fe^{+2}:O^{-2},Va} = -172\,728 + 89.109\,T$$

bcc, A2

$${}^0G^{Hbcc,A2}_{Fe} - {}^1H^{SER}_{Fe} = +GH^{SER}(Fe)$$

$${}^0G^{Hbcc,A2}_{O} - {}^1H^{SER}_{O} = 0.5G(O_2,GAS) + 30\,000$$

$${}^0L^{Hbcc,A2}_{Fe,O} = -209\,794 + 84T$$

$p = 0.4$

$${}^0T^{bcc,A2}_{CFe} = 1043$$

$${}^0\beta^{bcc,A2}_{Fe} = 2.22$$

fcc, A1

$${}^0G^{Hfcc,A1}_{Fe} - H^{SER}_{Fe} = +G(Fe,fcc)$$

$${}^0G^{Hfcc,A1}_{O} - H^{SER}_{O} = 0.5G(O_2,GAS) + 30\,0000$$

$${}^0L^{Hfcc,A1}_{Fe,O} = -199\,3455 + 84\,T$$

$p = 0.28$

$${}^0T^{fcc,A1}_{CFe} = -201$$

$${}^0\beta^{fcc,A1}_{Fe} = -2.1$$

Corundum

2 sublattices, sites 2:3

Constituents Fe:O

(continued)

Table 1 Assessed Parameters for the Fe-O System (cont.)

$${}^{0}G^{HCORUNDUM}_{Fe:O} - 2H^{SER}_{Fe} - 3H^{SER}_{O} = -858\,683 + 827.946T - 137.0089T\ln T + 1\,453\,810\ T^{-1}$$

$p = 0.28$

$${}^{0}T_{CFe:O}^{CORUNDUM} = -2867$$

$${}^{0}\beta_{Fe:O}^{CORUNDUM} = -25.1$$

Spinel

4 sublattices, sites 1 : 2 : 2 : 4

Constituents Fe^{+2}, Fe^{+3} : Fe^{+2}, Fe^{+3}, Va : Fe^{+2}, Va : O^{-2}

$${}^{0}G^{HSPINEL}_{Fe^{+2}:Fe^{+2}:Fe^{+2}:O^{-2}} - 5H^{SER}_{Fe} - 4H^{SER}_{O} = +9G(Fe_3O_4) + D(Fe_3O_4)$$

$${}^{0}G^{HSPINEL}_{Fe^{+3}:Fe^{+2}:Fe^{+2}:O^{-2}} - 5H^{SER}_{Fe} - 4H^{SER}_{O} = +9G(Fe_3O_4) + D(Fe_3O_4) - B(Fe_3O_4)$$

$${}^{0}G^{HSPINEL}_{Fe^{+2}:Fe^{+3}:Fe^{+2}:O^{-2}} - 5H^{SER}_{Fe} - 4H^{SER}_{O} = +9G(Fe_3O_4) + D(Fe_3O_4) - B(Fe_3O_4)$$

$${}^{0}G^{HSPINEL}_{Fe^{+3}:Fe^{+3}:Fe^{+2}:O^{-2}} - 5H^{SER}_{Fe} - 4H^{SER}_{O} = +9G(Fe_3O_4) + D(Fe_3O_4) - 2B(Fe_3O_4)$$

$${}^{0}G^{HSPINEL}_{Fe^{+2}:Va:Fe^{+2}:O^{-2}} - 3H^{SER}_{Fe} - 4H^{SER}_{O} = +7G(Fe_3O_4) + D(Fe_3O_4) - B(Fe_3O_4) + C(Fe_3O_4)$$

$${}^{0}G^{HSPINEL}_{Fe^{+3}:Va:Fe^{+2}:O^{-2}} - 3H^{SER}_{Fe} - 4H^{SER}_{O} = +7G(Fe_3O_4) + D(Fe_3O_4) - 2B(Fe_3O_4) + C(Fe_3O_4)$$

$${}^{0}G^{HSPINEL}_{Fe^{+2}:Fe^{+2}:Va:O^{-2}} - 3H^{SER}_{Fe} - 4H^{SER}_{O} = +7G(Fe_3O_4) - B(Fe_3O_4)$$

$${}^{0}G^{HSPINEL}_{Fe^{+3}:Fe^{+2}:Va:O^{-2}} - 3H^{SER}_{Fe} - 4H^{SER}_{O} = +7G(Fe_3O_4)$$

$${}^{0}G^{HSPINEL}_{Fe^{+2}:Fe^{+3}:Va:O^{-2}} - 3H^{SER}_{Fe} - 4H^{SER}_{O} = +7G(Fe_3O_4)$$

$${}^{0}G^{HSPINEL}_{Fe^{+3}:Fe^{+3}:Va:O^{-2}} - 3H^{SER}_{Fe} - 4H^{SER}_{O} = +7G(Fe_3O_4) - B(Fe_3O_4)$$

$${}^{0}G^{HSPINEL}_{Fe^{+2}:Va:Va:O^{-2}} - H^{SER}_{Fe} - 4H^{SER}_{O} = +5G(Fe_3O_4) + C(Fe_3O_4)$$

$${}^{0}G^{HSPINEL}_{Fe^{+3}:Va:Va:O^{-2}} - H^{SER}_{Fe} - 4H^{SER}_{O} = +5G(Fe_3O_4) - B(Fe_3O_4) + C(Fe_3O_4)$$

$p = 0.28$

$${}^{0}T_{C}^{SPINEL} = 848$$

$${}^{0}\beta^{SPINEL} = 44.54$$

Halite

2 sublattices, sites 1:1

Constituents Fe^{+2}, Fe^{+3}, Va : O^{-2}

$${}^{0}G^{HALITE}_{Fe^{+2}:O^{-2}} - H^{SER}_{Fe} - H^{SER}_{O} = +G(\text{wüstite})$$

$${}^{0}G^{HALITE}_{Fe^{+3}:O^{-2}} - H^{SER}_{Fe} - H^{SER}_{O} = +1.25G(\text{wüstite}) + 1.25A(\text{wüstite})$$

$${}^{0}G^{HALITE}_{Va:O^{-2}} - H^{SER}_{O} = 0$$

$${}^{0}L^{HALITE}_{Fe^{+2},Fe^{+3}:O^{-2}} = -12\,3244$$

$${}^{1}L^{HALITE}_{Fe^{+2},Fe^{+3}:O^{-2}} = -20\,0700$$

(continued)

Table 1 Assessed Parameters for the Fe-O System (cont.)

Functions

$G(\text{FeO,liq}) = -137\,387 + 225.42T - 37.2741T\ln T$

$G(\text{Fe,liq}) =$

$+GH^{SER}(\text{Fe}) + 12\,040.17 - 6.55843T - 3.6751551 \times 10^{-21}T^{7}$ for $298.15 < T < 1811.00$

$-10\,839.7 + 291.302T - 46T\ln T$ for $1811.00 < T < 6000.00$

$GH^{SER}(\text{Fe}) =$

$+1224.83 + 124.134T - 23.5143T\ln T - 0.00439752T^{2} - 5.89269 \times 10^{-8}T^{3} + 77\,358.3T^{-1}$ for $298.15 < T < 1811.00$

$-25\,384.451 + 299.31255T - 46T\ln T + 2.2960305 \times 10^{31}T^{-9}$ for $1811.00 < T < 6000.00$

$G(\text{Fe,fcc}) =$

$+GH^{SER}(\text{Fe}) - 1462.4 + 8.282T - 1.15T\ln T + 6.4 \times 10^{-4}T^{2}$ for $298.15 < T < 1811.00$

$-27\,098.266 + 300.25256T - 46T\ln T + 2.78854 \times 10^{31}T^{-9}$ for $1811.00 < T < 6000.00$

$G(Fe_3O_4) = -161\,731 + 144.873T - 24.9879T\ln T - 0.0011952256T^{2} + 206\,520T^{-1}$

$G(O_2,\text{gas}) =$

$-6\,961.74451 - 76\,729.7484T^{-1} - 51.0057202T - 22.2710136T\ln T - 0.0101977469T^{2} + 1.32369208 \times 10^{-6}T^{3}$ for $298.15 < T < 1000.00$

$-13\,137.5203 + 525809.556T^{-1} + 25.3200332T - 33.627603T\ln T - 0.00119159274T^{2} + 1.35611111 \times 10^{-8}T^{3}$ for $1000.00 < T < 3300.00$

$-27\,973.4908 + 8\,766\,421.4T^{-1} + 62.5195726T - 37.9072074T\ln T - 8.50483772 \times 10^{-4}T^{2} + 2.14409777 \times 10^{-8}T^{3}$ for $3300.00 < T < 6000.00$

$D(Fe_3O_4) = +402\,520 - 30.529T$

$B(Fe_3O_4) = +46\,826 - 27.266T$

$C(Fe_3O_4) = +120\,730 - 20.102T$

$G(\text{wüstite}) = -279\,318 + 252.848T - 46.12826T\ln T - 0.0057402984T^{2}$

$A(\text{wüstite}) = -55\,384 + 27.888T$

For the fcc and bcc phase, a substitutional regular-solution model was applied with the following Gibbs energy expression:

$$\Delta_{mix}G = X_{Fe}G^{0}_{Fe} + X_{O}G^{0}_{O} + RT[X_{Fe}\ln(X_{Fe}) + X_{O}\ln(X_{O})] + X_{Fe}X_{O}L_{Fe,O} \qquad \text{(Eq 1)}$$

where X_{Fe} and X_O are the mole fraction of iron and oxygen, respectively and G^0_{Fe} and G^0_O are the Gibbs energies of pure iron and oxygen, respectively. The term multiplied with RT is the ideal entropy of mixing, and the last term is the regular-solution interaction term.

The magnetic properties of the bcc phase for pure Fe were described using a model proposed by Inden[40] and simplified by Hillert and Jarl[41] and Chin *et al.*[42] The description of pure iron was taken from the assessment by Fernandez and Gustafson.[43]

Halite Phase (Wüstite)

Halite is stable from about 830 to 1700 K and has a considerable solid solubility. Already in equilibrium with the iron phases, its composition is markedly hyperstoichiometric, with respect to Fe with the approximate formula $Fe_{0.947}O$. With higher oxygen potentials and higher temperatures, it remains stable up to X_O = 0.55 ($Fe_{0.818}O$) at 1700 K. This is due to the fact that iron has two valency states, Fe^{+2} and Fe^{+3}, and the fraction of Fe^{+3} increases with the oxygen potential. The ideal structure of halite is simple, with the oxygen ions forming an fcc lattice and the iron ions on the octahedral interstitial sites. To accommodate the trivalent iron ions, vacant sites are formed in the octahedral sublattice. The model applied to halite takes this into account by using two sublattices with the following structure:

$$(Fe^{+2}, Fe^{+3}, Va)_1(O^{-2})_1$$

This structure can be represented in a constitutional triangle, as shown in Fig. 1. In this triangle, one corner represents stoichiometric FeO, whereas the other two represent hypothetical compounds with a net charge, FeO^{+1} and O^{-2}. Only the solid line through the triangle has any physical significance, as it represents the neutral combination of Fe^{+3} and Va, *i.e.* where the fraction of vacancies is half that of Fe^{+3}.

The compound energy model proposed by Hillert *et al.*[44] gives the following expression for the Gibbs energy:

$$\Delta_{mix}G = {}_{y2}G^0_{20} + y_3 G^0_{30} + y_V G_{VO} + RT[y_2 \ln(y_2) + y_3 \ln(y_3) + y_V \ln(y_V)] + \Delta_{mix}G^{ex} \quad \text{(Eq 2)}$$

where the variables y_2 and y_3 are the fraction of sites in the metallic sublattice occupied by divalent and trivalent iron respectively, and y_V is the fraction of vacant sites. The y fraction variables are usually called site fractions. The notation y_2 rather than $y_{Fe^{+2}}$ is for convenience.

The three G terms describe the Gibbs energies of the three corners of Fig. 1; as two corners have a net charge, it is possible to evaluate a neutral combination of these only. The parameter G^0_{VO} represents a halite phase with only oxygen, and this parameter will be used in other oxide systems where halite is stable also. Therefore it is convenient to set it to zero, $G^0_{VO} = 0$. The term preceded by RT is the ideal entropy of mixing in the metallic sublattice. The sublattice with oxygen has no entropy of mixing, as it is completely filled with O^{-2}.

The excess Gibbs energy, $\Delta_{mix}G^{ex}$, for the halite can be described with Redlich-Kister expressions, and restricting this to two terms we have:

$$\Delta_{mix}G^{ex} = y_2y_3[L^0_{2,3:O} + (y_2 - y_3)L^1_{2,3:O}] + y_2y_V[L^0_{2,V:O} + (y_2 - y_V)L^1_{2,V:O}] + y_3y_V[L^0_{3,V:O} + (y_3 - y_V)L^1_{3,V:O}] \quad \text{(Eq 3)}$$

In the interaction parameters, a colon (:) is used to separate constituents in different sublattices, whereas a comma (,) is used to separate constituents in the same sublattice.

There are two Redlich-Kister terms form each side of the triangle in Fig. 1. However, as the vacancies are needed just to maintain electroneutrality, the parameters involving vacancies should be set to zero. One may otherwise have problems when combining assessments of the halite phase from different subsystems. The Fe-O system is not a good example of this, but consider the solubility of Si in periclase (MgO), which can be modeled in the same way with two sublattices $(Mg^{+2}, Si^{+2}, Va)(O^{-2})$. If a parameter $L_{Si^{+4},Va:O^{+2}}$ were assessed in this system, this parameter would appear also in lime (CaO) when assessing the $CaO\text{-}SiO_2$ system, because the parameter involves only Si, vacancies, and oxygen. As these binary systems can be assessed independently, it is evident that all parameters involving vacancies, introduced for electroneutrality, should be zero.

The mole fraction can be calculated from the site fraction using the following formula:

$$X_{Fe} = \frac{y_2 + y_3}{1 + y_2 + y_3} \quad \text{(Eq 4a)}$$

$$X_O = \frac{1}{1 + y_2 + y_3} \quad \text{(Eq 4b)}$$

The maximum value for y_3 is 2/3, and the model for the halite phase can thus describe the composition range for x_O from 0.5 to 0.6.

Spinel (Magnetite)

Magnetite is a spinel with an ideal stoichiometry Fe_3O_4. The spinel structure has oxygen ions in an fcc sublattice, with divalent and trivalent metallic ions in the octahedral and tetrahedral interstitial sublattices. The number of sites on the octahedral sublattice is equal to that of oxygen sites, whereas the tetrahedral sublattice has twice as many sites. In a spinel, only half the octahedral sites and one eighth of the tetrahedral sites are occupied. A normal spinel has the trivalent ions on the octahedral sites and the divalent ions on the tetrahedral sites. However, at low temperatures, magnetite is an inverse spinel, with the tetrahedral sites filled with Fe^{+3} and with both Fe^{+2} and Fe^{+3} on the octahedral sites. At higher temperatures, magnetite transforms gradually into a normal spinel, and before melting, it is almost random. The structure of the stoichiometric magnetite is thus:

$$(Fe^{+3}, Fe^{+2})_1(Fe^{+3}, Fe^{+2})_2(O^{-2})_4$$

However, magnetite also has a considerable deviation from its ideal stoichiometry at higher oxygen potentials and temperatures. This can easily be accommodated in the structure above by allowing an excess of Fe^{+3} on the octahedral sites and at the same time introducing vacancies to maintain electroneutrality. The modified structure would be:

$$(Fe^{+3}, Fe^{+2})_1(Fe^{+3}, Fe^{+2}, Va)_2(O^{-2})_4$$

Finally, magnetite has a small deviation toward excess iron in equilibrium with wüstite and with liquid at high temperatures. This is due to some Fe^{+2} entering as interstitials into the remaining octahedral sites that are normally empty. To model this, we add one more sublattice with two sites that are filled mainly with vacancies:

$$(Fe^{+2}, Fe^{+3})_1(Fe^{+2}, Fe^{+3}, Va)_2(Fe^{+2}, Va)_2(O^{-2})_4$$

The compound energy model when applied to this structure was discussed by Hillert *et al.*,[44] and the Gibbs energy expression is a straightforward but long expression with 12 G^0 terms, most of which represent compounds that have a net charge:

$$\begin{aligned}\Delta_{mix}G = {} & y_2^T y_2^O y_2^I G^0_{222O} + y_2^T y_2^O y_V^I G^0_{22VO} + y_3^T y_2^O y_2^I G^0_{322O} \\ & + y_3^T y_2^O y_V^I G^0_{32VO} + y_2^T y_3^O y_2^I G^0_{232O} \\ & + y_2^T y_3^O y_V^I G^0_{23VO} + y_3^T y_3^O y_2^I G^0_{332O} \\ & + y_3^T y_3^O y_V^I G^0_{33VO} + y_2^T y_V^O y_2^I G^0_{2V2O} \\ & + y_2^T y_V^O y_V^I G^0_{2VVO} + y_3^T y_V^O y_2^I G^0_{2V2O} \\ & + y_3^T y_V^O y_V^I G_{3VVO} + RT\,[(y_2^T \ln (y_2^T) + y_3^T \ln (y_3^T)] \\ & + 2[y_2^O \ln (y_2^O) + y_3^O \ln (y_3^O) + y_V^O \ln (y_V^O)] \\ & + 2[y_2^I \ln (y_2^I) + y_V^I \ln (y_V^I)] \qquad \text{(Eq 5)}\end{aligned}$$

where the superscript T means the tetrahedral sublattice, O the octahedral sublattice and I the interstitial sublattice. The subscripts 2, 3, and V mean divalent iron, trivalent iron, and vacancies, respectively.

The parameter G^0_{23VO} represents a neutral compound and is identical to a normal spinel, whereas most of the others represent compounds with a net charge and can be assigned values only in neutral combinations. There are several alternative ways to establish such combinations, and, following Hillert *et al.*,[44] we will first consider stoichiometric magnetite. In this case, we have only four parameters G^0_{xxVO}, where x can be 2 or 3. At equilibrium, the following equation describes the ordering:

$$\begin{aligned}0.5(G^0_{22VO} + G^0_{23VO} - 2G^0_{32VO}) + y_2^T(G^0_{23VO} + G^0_{32VO} \\ G^0_{22VO} - G^0_{33VO}) = RT \ln \left(\frac{y_3^T y_2^O}{y_2^T y_3^O} \right) \qquad \text{(Eq 6)}\end{aligned}$$

From the experiments by Wu and Mason,[26] one finds that the right-hand side of Eq 6 can be described by a temperature-dependent function that is independent of the order. This means that the second term can be put to zero:

$$G^0_{23VO} - G^0_{33VO} = G^0_{22VO} - G^0_{32VO} \qquad \text{(Eq 7)}$$

This relation can be given the interpretation that the energy for an exchange from an Fe^{+2} to an Fe^{+3} ion in the tetrahedral sublattice is independent of whether the octahedral sublattice is filled with Fe^{+2} or Fe^{+3}. We still have three independent parameters, but we may put an arbitrary value to any one of the parameters representing a charged compound. In this case, we instead chose to put:

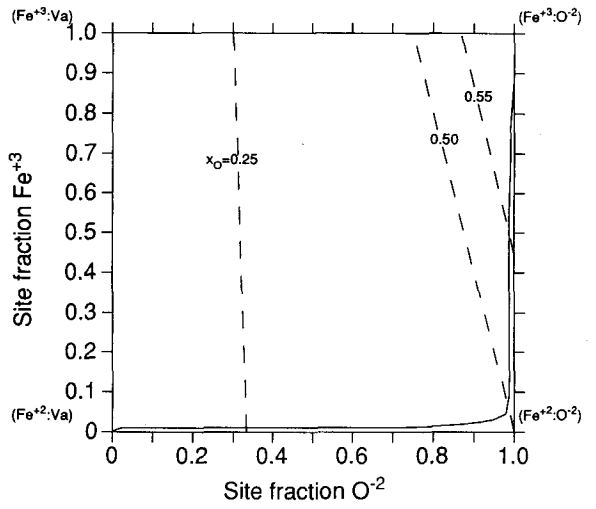

Fig. 2 Structural model of Fe-O liquid. The liquid has an internal degree of freedom because iron can be either Fe^{+2} or Fe^{+3}. The dashed lines represent iso-concentration lines for oxygen with the mole fraction given by the numbers. The Gibbs energy expression for the liquid must be minimized in order to find the fraction of Fe^{+3} which gives the lowest Gibbs energy for each composition. The bottom left corner represents pure liquid iron. The fraction of Fe^{+3} will be very small going from pure iron up to an oxygen mole fraction close to 0.5 and thus one will follow the bottom side of the square. On this side the liquid has a miscibility gap. At higher oxygen content the fraction of Fe^{+3} will increase until the top right corner is reached. The full line gives a rough picture of this variation. Note that the model for the liquid ends at $X_O = 0.6$.

$$G^0_{32VO} = G^0_{23VO} \qquad \text{(Eq 8)}$$

If we now extend the description to nonstoichiometric spinel, we may use the relation in Eq 7 as a general rule to find relations between the other parameters also. Thus, we chose a similar relation when the octahedral sublattice is filled with vacancies:

$$G^0_{2VVO} - G^0_{3VVO} = G^0_{22VO} - G^0_{32VO} \qquad \text{(Eq 9)}$$

The deviation from stoichiometry toward higher oxygen content can be described by the formation of octahedral vacancies. Assuming that the energy to create an octahedral vacancy is independent of the ion in the tetrahedral sublattice we have:

$$G^0_{2VVO} - G^0_{23VO} = G^0_{2VVO} - G^0_{33VO} \qquad \text{(Eq 10)}$$

We may here select G^0_{2VVO} as the parameter describing the tendency to form vacancies. The deviation toward lower oxygen content can be described by interstitial Fe^{+2} ions on the extra octahedral sites. We obtain the following relations with the same assumption as in Eq 7:

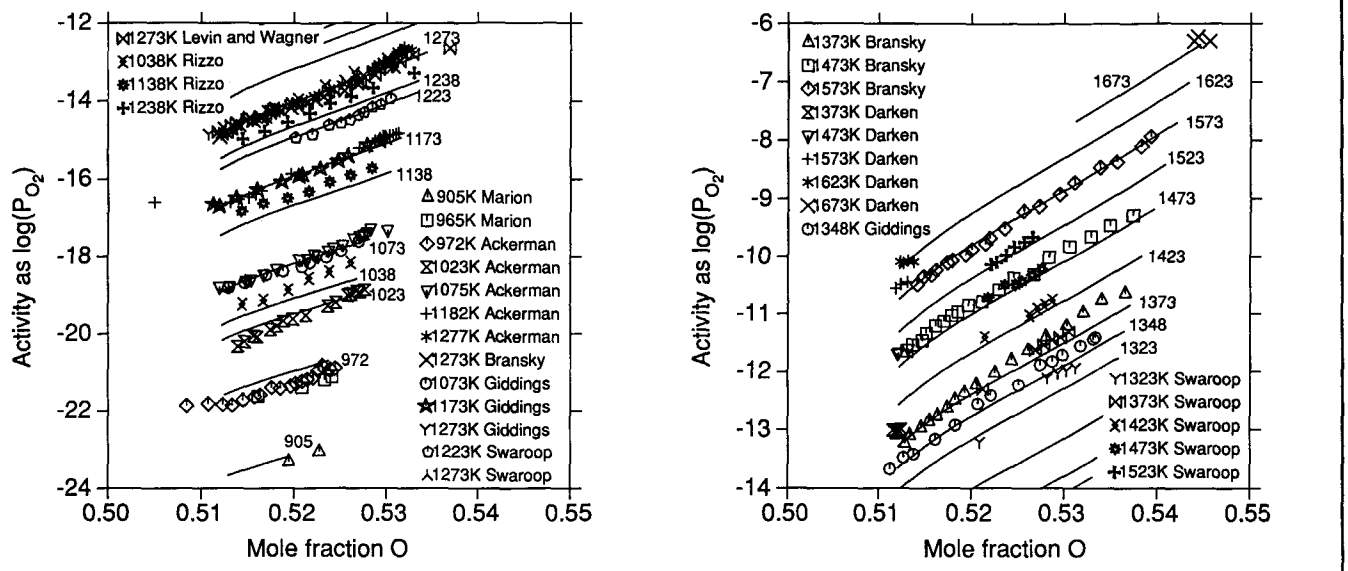

Fig. 3 Calculated vs experimental oxygen activity in halite. The lines show how the calculated oxygen activities, expressed as $\log(P_{O_2})$, varies with oxygen content in the halite phase field at various temperatures. The temperature for each line is given in the figure.

$$G^0_{22VO} - G^0_{22VO} = G^0_{232O} - G^0_{23VO} = G^0_{2V2O} - G^0_{2VVO}$$
$$= G^0_{322O} - G^0_{32VO} = G^0_{332O} - G^0_{33VO}$$
$$= G^0_{3V2O} - G^0_{3VVO} \qquad \text{(Eq 11)}$$

By selecting G^0_{222O} as the independent variable describing the formation of interstitials, we can express the remaining eight parameters in the four independent parameters using Eq 7 to 11. The final relations are:

G^0_{2VVO} = independent
G^0_{22VO} = independent
G^0_{23VO} = independent
$G^0_{3VVO} = G^0_{2VVO} - G^0_{22VO} + G^0_{23VO}$
$G^0_{32VO} = G^0_{23VO}$
$G^0_{33VO} = 2G_{23VO} - G^0_{22VO}$
$G^0_{2V2O} = G^0_{222O} - G^0_{22VO} + G^0_{2VVO}$
G^0_{222O} = independent
$G^0_{232O} = G_{222O} - G^0_{22VO} + G^0_{23VO}$
$G^0_{3V2O} = G^0_{222O} - 2G^0_{22VO} + G^0_{2VVO} + G^0_{23VO}$
$G^0_{322O} = G^0_{222O} - G^0_{22VO} + G^0_{23VO}$
$G^0_{332O} = G^0_{222O} - 2G^0_{22VO} + 2G^0_{23VO}$ (Eq 12)

The spinel is ferromagnetic at room temperature and has a magnetic transition at 848 K. The magnetic contribution to the Gibbs energy is described using the same formalism that Inden[40] suggested for bcc iron. The magnetic moment that is needed in the model was evaluated using experimental data on the heat capacity and enthalpy.

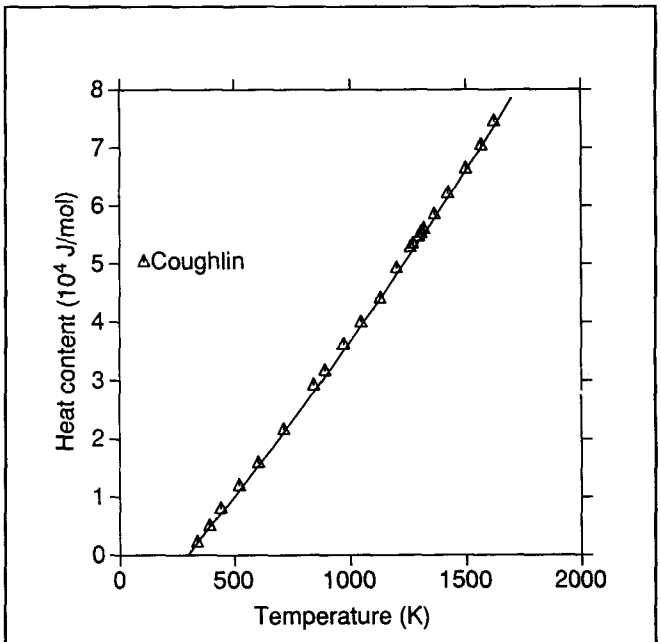

Fig. 4 Calculated vs experimental heat capacity of halite ($Fe_{0.947}O$).

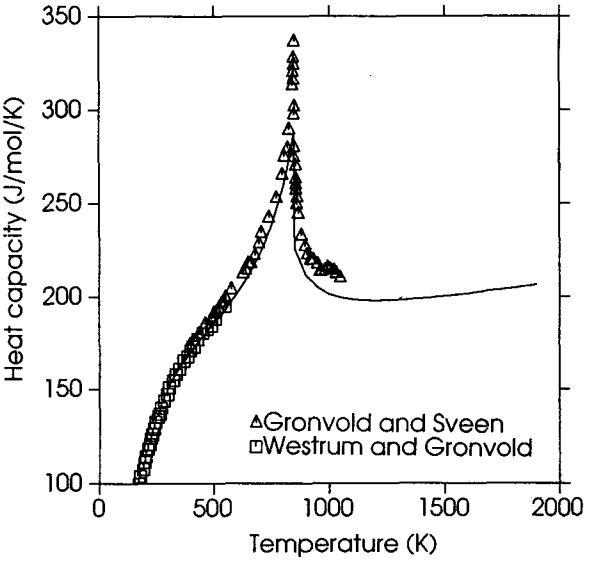

Fig. 5 Calculated vs Experimental Heat Capacity of Spinel (Fe_3O_4).

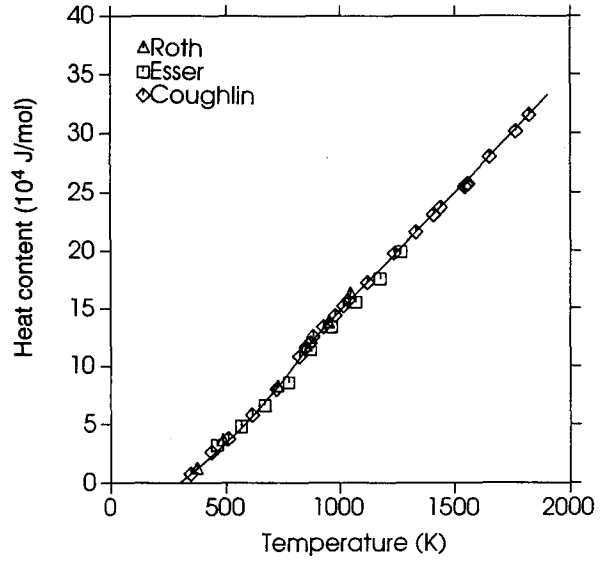

Fig. 6 Calculated vs Experimental Enthalpy of Spinel (Fe_3O_4).

Corundum (Hematite)

The hematite composition is very close to stoichiometric Fe_2O_3 at all temperatures, and it was treated as a stoichiometric compound in this assessment. There is a lambda anomaly in the corundum heat capacity at 943 K, which was described using the same magnetic model as for magnetite. Hematite has a hexagonal structure and is isomorphous with, for example, Al_2O_3 (corundum) and Cr_2O_3.

Liquid

The liquid phase is characterized by a large miscibility gap between metallic liquid iron and liquid oxide. The solubility of oxygen in the metallic liquid is small, but the liquid oxide extends from $X_O = 0.5$ to $X_O = 0.58$. The ionic two-sublattice model developed recently by Hillert *et al.*[45] was adopted for the description of the liquid. This model is similar to the model used for molten salts, with one sublattice for anions and one for cations, but is extended to allow hypothetical vacancies, with an induced charge, and neutral atoms in the anion sublattice. In this way, one may use the same model for both the metallic liquid and the oxide liquid. In the Fe-O system, considering Fe^{+2}, Fe^{+3}, O^{-2}, and vacancies, we obtain this model:

$$(Fe^{+2}, Fe^{+3})_P(O^{-2}, Va^{-Q})_Q$$

According to the model, the stoichiometric factors P and Q vary with the composition to make the phase electrically neutral. The formula for this is:

$$P = \sum_i y_i(-v_i) + y_{Va}Q$$

$$Q = \sum_j y_j v_j \qquad \text{(Eq 13)}$$

where v_i is the valency of ion i. The summation over i is made for all anions, *i.e.*, charged constituents in the second sublattice, and the summation over j is made for all cations, *i.e.*, the constituents in the first sublattice. The vacancies have an induced charge equal to the average charge of the cation sublattice, *i.e.*, the induced charge is equal to the number of sites. This follows from the requirement that when there is no oxygen present, the model should become identical to a substitutional regular-solution model between metallic atoms. Fe-O is slightly peculiar, because Fe^{+2} and Fe^{+3} are two different valency states of the same atom. In the model, these are treated as different constituents, and one will obtain a contribution to the entropy of mixing from these constituents. Further, the hypothetical vacancies will contribute to the entropy in the anion sublattice.

In Fig. 2, the constitutional square for this phase is shown. The dashed lines are equicompositional lines along which the oxygen content is the same. The model thus has an internal degree of freedom due to the fact that Fe has two valency states. The parameters assessed for the liquid phase will determine the state of lowest Gibbs energy for each composition. The solid line in the diagram gives the approximate constitution of the stable liquid, using the assumption that the liquid at the composition FeO should consist mainly of Fe^{+2} and O^{-2} and very little Fe^{+3}.

The Gibbs energy expression used for the liquid is:

$$\begin{aligned}\Delta_{mix}G = {} & y_2y_O\,G^0_{Fe_2O_2} + y_3y_O\,G^0_{Fe_2O_3} \\ & + Q(y_2y_V\,G^0_{Fe^{+2}:Va^{-2}} + y_3y_V\,G^0_{Fe^{+3}:Va^{-3}}) \\ & + RTP[y_2\ln(y_2) + y_3\ln(y_3))] + RTQ[(y_O\ln(y_O) \\ & + y_V\ln(y_V)] + \Delta_{mix}G^{ex}\end{aligned} \qquad \text{(Eq 14)}$$

Note that P and Q depend on the composition as given by Eq 13. The first four terms are the Gibbs energies of formation of the

Table 2 Calculated Thermochemical Properties of Wüstite ($Fe_{0.947}O$)
$\Delta_f H(298.15) = -265\,152$ J/mol

Temperature, K	C_p, J/mol·K	$H-H(298.15)$, J/mol	S, J/mol·K	G, J/mol
298.15	48.2381	0	58.734	-282 664
350	48.8176	2 516.2	66.514	-285 916
400	49.3764	4 971.0	73.069	-289 409
450	49.9352	7 453.8	78.917	-293 211
500	50.4940	9 964.5	84.207	-297 292
550	51.0529	12 503.2	89.046	-301 625
600	51.6117	15 069.8	93.512	-306 190
650	52.1705	17 664.4	97.665	-310 971
700	52.7293	20 286.9	101.552	-315 952
750	53.2881	22 937.3	105.209	-321 122
800	53.8469	25 615.7	108.666	-326 470
850	54.4058	28 322.0	111.947	-331 986
900	54.9646	31 056.3	115.073	-337 662
950	55.5234	33 818.5	118.059	-343 491
1000	56.0822	36 608.6	120.922	-349 466
1050	56.6410	39 426.7	123.671	-355 581
1100	57.1999	42 272.7	126.319	-361 831
1150	57.7587	45 146.7	128.874	-368 211
1200	58.3175	48 048.6	131.344	-374 717
1250	58.8763	50 978.4	133.736	-381 344
1300	59.4351	53 936.2	136.056	-388 089
1350	59.9939	56 921.9	138.310	-394 949
1400	60.5528	59 935.6	140.502	-401 919
1450	61.1116	62 977.2	142.636	-408 998
1500	61.6704	66 046.8	144.717	-416 182
1550	62.2292	69 144.3	146.749	-423 469
1600	62.7880	72 269.7	148.733	-430 856
1650	63.3469	75 423.1	150.674	-438 342
1700	63.9057	78 604.4	152.573	-445 923

corners in the reciprocal system. $G^0_{Fe^{+2}:Va}$ and $G^0_{Fe^{+3}:Va}$ both represent pure iron liquid and both values should be for 1 mole of atoms, whereas $G^0_{Fe_2O_2}$ is for 4 moles of atoms, and $G^0_{Fe_2O_3}$ is for 5 moles of atoms. The terms multiplied with RTP and RTQ, where R is the gas constant and T the absolute temperature, are the ideal entropies of mixing for the cation and anion sublattice, respectively. Finally the excess Gibbs energy term, $\Delta_{mix}G^{ex}$ restricting the model to two Redlich-Kister terms, is:

$$\begin{aligned}\Delta_{mix}G = {} & y_2y_3y_V[L^0_{2,3:V} + (y_2 - y_3)L^1_{2,3:V}] \\ & + y_2y_3y_O[L^0_{2,3:O} + (y_2 - y_3)L^1_{2,3:O}] \\ & + y_2y_Oy_V[L^0_{2:O,V} + (y_O - y_V)L^1_{2:O,V}] \\ & + y_3y_Oy_V[L^0_{3:O,V} + (y_O - y_V)L^1_{3:O,V}] \end{aligned} \quad \text{(Eq 15)}$$

There are two Redlich-Kister terms from each side of the square. However, in the reciprocal system, the two sides Fe^{+2}:Va – Fe^{+3}:Va and Fe^{+3}:Va – Fe^{+3}:O^{-2} cannot be evaluated because the stable liquid phase will follow very close to the other two sides, as demonstrated in Fig. 2. Thus the interaction parameters for these sides were put to zero. The remaining four interaction parameters were used to fit the experimental data.

Assessment Procedure

The assessment was made using the computer software PARROT developed by Jansson,[46] included in the Thermo-Calc databank system.[47]

For the fcc and bcc phases, Gibbs energies of formation of oxygen in the fcc and the bcc structures were estimated, and an interaction parameter was determined in each phase. These were actually the last parameters evaluated after all other parameters had been determined. The values are listed in Table 1.

Halite

The assessment procedure started with describing the oxygen potential in the halite phase field. The oxygen activity is almost linearly dependent on the oxygen content in the stable range. From the model, the oxygen potential must be calculated as the difference between Fe_2O_3 and FeO:

$$G_{O_2} = 2G_{Fe_2O_3} - 4G_{FeO} \quad \text{(Eq 16)}$$

From the model, we can obtain $G_{Fe_2O_3}$ as a weighted average of the chemical potentials between the two corners $G_{Fe^{+3}:O^{-2}}$ and $G_{Va:O^{-2}}$ in Fig. 1:

$$G_{Fe_2O_3} = 2G_{Fe^{+3}:O^{-2}} + G_{Va:O^{-2}} \quad \text{(Eq 17)}$$

We can thus calculate the oxygen potential by combining the chemical potentials from the three corners of Fig. 1. The chemical potential of one corner can be calculated by the general formula for a phase with sublattices:

$$G_{A:B} = G_{mix} + \frac{\partial G_{mix}}{\partial y_A} + \frac{\partial G_{mix}}{\partial y_B} - \sum_i y_i \frac{\partial G_{mix}}{\partial y_i} \quad \text{(Eq 18)}$$

Inserting Eq 17 and 18 in Eq 16 yields:

Table 3 Calculated Thermochemical Properties of Magnetite (Fe_3O_4)
$\Delta_f H(298) = -1\,115\,877$ J/mol

Temperature, K	C_p, J/mol·K	$H-H(298.15)$, J/mol	S, J/mol·K	G, J/mol
298.15	150.249	0	145.804	−1 159 210
350	161.852	8 136	170.930	−1 167 570
400	170.541	16 519	193.302	−1 176 680
450	178.177	25 359	214.117	−1 186 870
500	185.540	34 637	233.661	−1 198 070
550	193.169	44 355	252.178	−1 210 220
600	201.531	54 531	269.880	−1 223 270
650	211.159	65 201	286.956	−1 237 200
700	222.814	76 432	303.596	−1 251 960
750	237.763	88 340	320.022	−1 267 550
800	258.267	101 130	336.523	−1 283 960
848	287.021	114 570	352.830	−1 300 510
850	225.761	115 039	353.383	−1 301 210
900	211.462	126 326	366.289	−1 319 210
950	204.932	137 111	377.953	−1 337 820
1000	201.494	147 642	388.757	−1 356 990
1050	199.569	158 025	398.890	−1 376 690
1100	198.504	168 317	408.466	−1 396 870
1150	197.979	178 553	417.566	−1 417 520
1200	197.815	188 755	426.250	−1 438 620
1250	197.904	198 938	434.564	−1 460 140
1300	198.174	209 116	442.548	−1 482 070
1350	198.578	219 297	450.232	−1 504 390
1400	199.082	229 487	457.644	−1 527 090
1450	199.661	239 692	464.806	−1 550 150
1500	200.297	249 917	471.739	−1 573 570
1550	200.978	260 166	478.460	−1 597 320
1600	201.693	270 441	484.984	−1 621 410
1650	202.435	280 745	491.326	−1 645 820
1700	203.199	291 081	497.497	−1 670 540
1750	203.979	301 450	503.508	−1 695 570
1800	204.772	311 854	509.370	−1 720 890
1850	205.575	322 295	515.091	−1 746 500
1900	206.388	332 773	520.680	−1 772 400

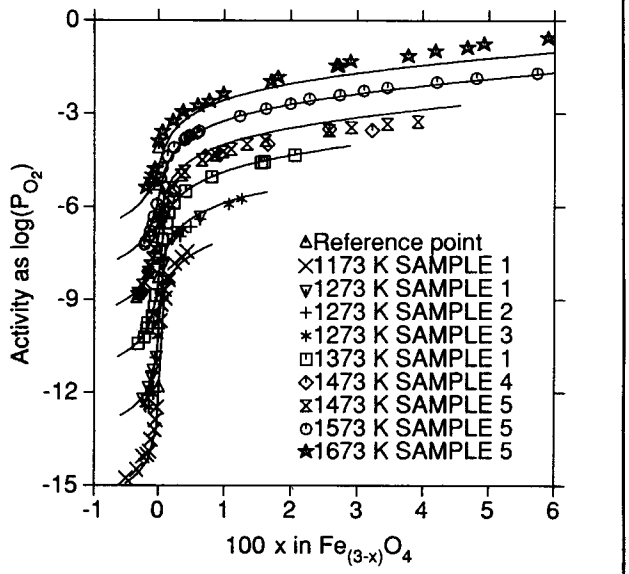

Fig. 7 Calculated vs experimental oxygen potential in spinel vs composition.

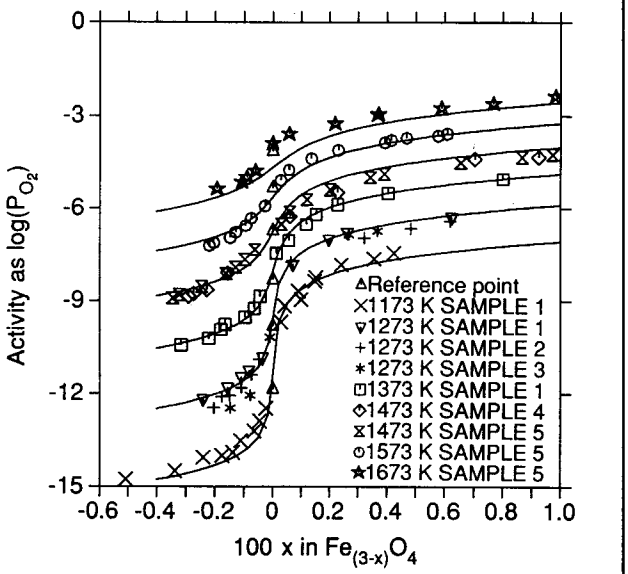

Fig. 8 Calculated and experimental oxygen potential near stoichiometric spinel vs composition.

$$G_{O_2} = 4(G_{mix} + \frac{\partial G_{mix}}{\partial y_3} - \sum_i y_i \frac{\partial G_{mix}}{\partial y_i} + 2(G_{mix} + \frac{\partial G_{mix}}{\partial y_V} - \sum_i y_i \frac{\partial G_{mix}}{\partial y_i}) - 4\,(G_{mix} + \frac{\partial G_{mix}}{\partial y_2} - \sum_i y_i \frac{\partial G_{mix}}{\partial y_i})$$
$$= 2G_{mix} + 4\frac{\partial G_{mix}}{\partial y_3} + 2\frac{\partial G_{mix}}{\partial y_V} - 4\frac{\partial G_{mix}}{\partial y_2} - 2\sum_{i=2,3,V} y_i \frac{\partial G_{mix}}{\partial y_i} \quad \text{(Eq 19)}$$

Inserting Eq 2 and 3 in Eq 19 and using $G_V = 0$ yields:

$$G_{O_2} = 4\left(G^0_3 - G^0_2\right) + RT \ln\left(\frac{y_3^4 y_V^2}{y_2^4}\right) + 2(2y_2 - 2y_3 - y_2y_3)(L^0_{2,3,:O} + (y_2 - y_3)L^1_{2,3:O}) - y_2y_3(8 + y_2 - y_3)L^1_{2,3:O} \quad \text{(Eq 20)}$$

We find that only the difference $G^0_3 - G^0_2$ influences the oxygen potential. The assessed values for this difference and of the regular and subregular interaction parameters for the halite are given in Table 1. In Fig. 3 the calculated activities are compared with experimental data on the oxygen activity in the wüstite. The lines have been calculated from Eq 20, and the agreement is good.

The value of G^0_2 was determined using the experimental values of the heat capacity and enthalpy. The estimated values of $S(298)$ and $\Delta_f H(298)$ were also used in the assessment. In Table 2, the calculated values for the thermochemical properties of a halite with composition $Fe_{0.947}O$ are tabulated. In Fig. 4, the enthalpy of halite relative to 298.15 K is plotted. The heat capacity was assumed to be independent of composition.

No attempt was made to describe the reported lambda anomaly in the heat capacity for metastable halite below 298.15 K.

Spinel

The spinel was assessed in two steps also. First, a parameter describing stoichiometric Fe_3O_4 was determined against experimental data on the heat capacity and enthalpy. The magnetic transition was fixed to the experimental value 848 K, but the Bohr magneton number, ${}^0\beta$, was used as a parameter to fit the shape of the lambda transition.

The final value of the Bohr magneton number, ${}^0\beta = 44.54$, may seem uncharacteristically large, but is due to a peculiarity in the implementation of the magnetic model. The Bohr magneton number used in the model is an average value per atom, and the model does not allow considering individual ${}^0\beta$ of the constituents of the phase. Further, the value is valid for a phase with seven atoms, and this has to be incorporated in the ${}^0\beta$ value used in the term $\ln({}^0\beta + 1)$, as the number of atoms per formula units of the phase does not enter into the expression for the magnetic contribution. If $\ln({}^0\beta + 1)$ had been multiplied with the number of atoms in 1 mole of the phase, the value of ${}^0\beta$ would be more realistic, but that does not change the model. The value of ${}^0\beta$ per atom could be calculated from the following formula ${}^0\beta = (44.54 + 1)^{(1/7)} - 1 = 1.7$, if oxygen and iron had the same Bohr magneton number. If only the iron atoms contributed to the Bohr magneton number, the value per iron atoms would be equal to 3.6.

The experimental data on the variation of the oxygen potential and degree of order was then used to evaluate the ordering of Fe^{+2}

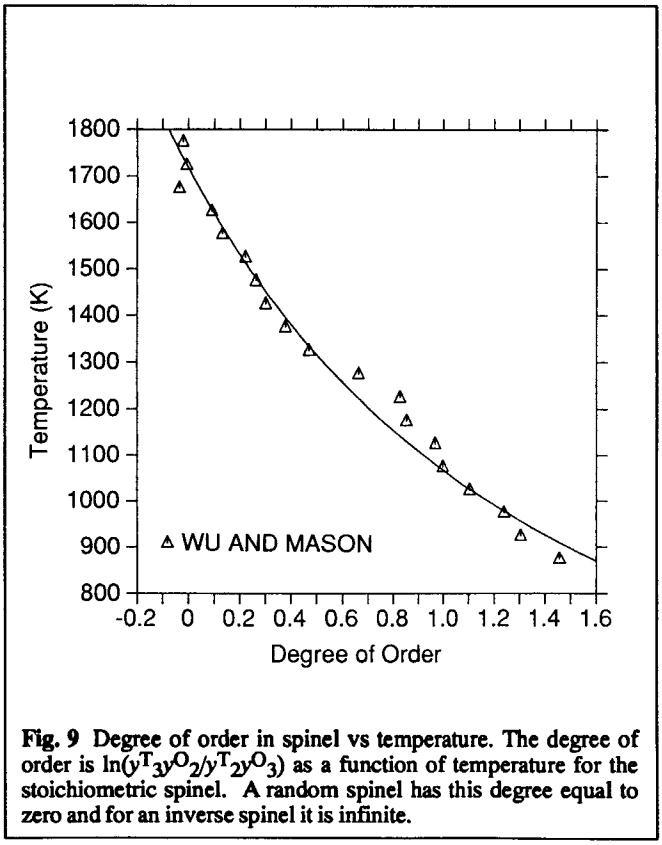

Fig. 9 Degree of order in spinel vs temperature. The degree of order is $\ln(y^{T_3}y^{O_2}/y^{T_2}y^{O_3})$ as a function of temperature for the stoichiometric spinel. A random spinel has this degree equal to zero and for an inverse spinel it is infinite.

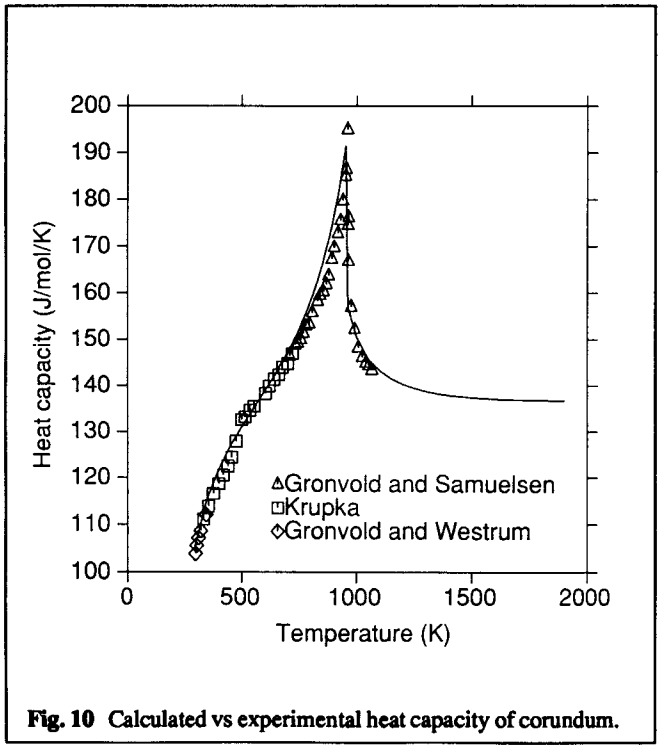

Fig. 10 Calculated vs experimental heat capacity of corundum.

Table 4 Calculated Thermochemical Properties of Hematite (Fe_2O_3)
$\Delta_f H(298) = -823\ 287$ J/mol

Temperature, K	C_p, J/mol·K	$H-H(298.15)$, J/mol	S, J/mol·K	G, J/mol
298.15	105.483	0	87.832	-849 474
350	115.188	5 738	105.557	-854 493
400	121.697	11 668	121.385	-860 172
450	126.732	17 883	136.020	-866 612
500	130.995	24 329	149.597	-873 756
550	134.913	30 977	162.268	-881 557
600	138.775	37 819	174.172	-889 970
650	142.810	44 858	185.437	-898 963
700	147.242	52 107	196.180	-908 506
750	152.337	59 593	206.507	-918 574
800	158.475	67 358	216.528	-929 151
850	166.255	75 468	226.359	-940 224
900	176.681	84 027	236.141	-951 786
950	191.478	93 208	246.065	-963 840
955	193.298	94 170	247.075	-965 073
1000	150.465	101 121	254.189	-976 355
1050	145.883	108 519	261.408	-989 247
1100	143.203	115 741	268.128	-1 002 490
1150	141.465	122 854	274.453	-1 016 050
1200	140.262	129 896	280.447	-1 029 930
1250	139.395	136 886	286.154	-1 044 090
1300	138.752	143 839	291.608	-1 058 540
1350	138.267	150 764	296.835	-1 073 250
1400	137.897	157 668	301.856	-1 088 220
1450	137.611	164 555	306.690	-1 103 430
1500	137.390	171 430	311.351	-1 118 880
1550	137.217	178 295	315.854	-1 134 570
1600	137.083	185 152	320.208	-1 150 470
1650	136.978	192 004	324.424	-1 166 580
1700	136.895	198 850	328.512	-1 182 910
1750	136.831	205 694	332.480	-1 199 430
1800	136.782	212 534	336.334	-1 216 150
1850	136.744	219 372	340.081	-1 233 060
1900	136.715	226 208	343.727	-1 250 160

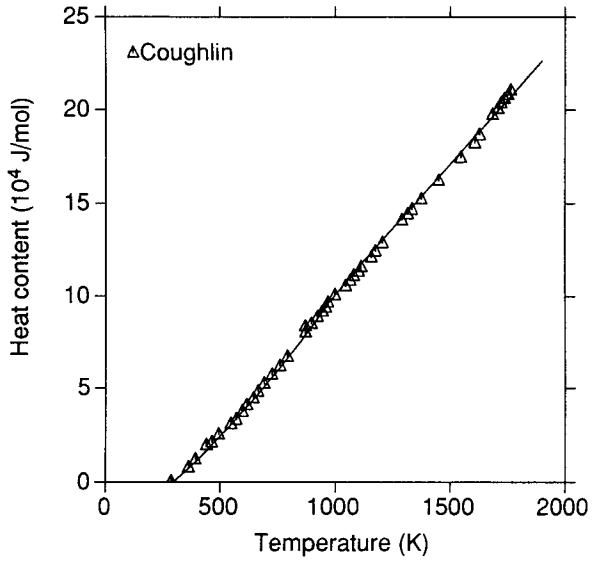

Fig. 11 Calculated vs experimental enthalpy of corundum.

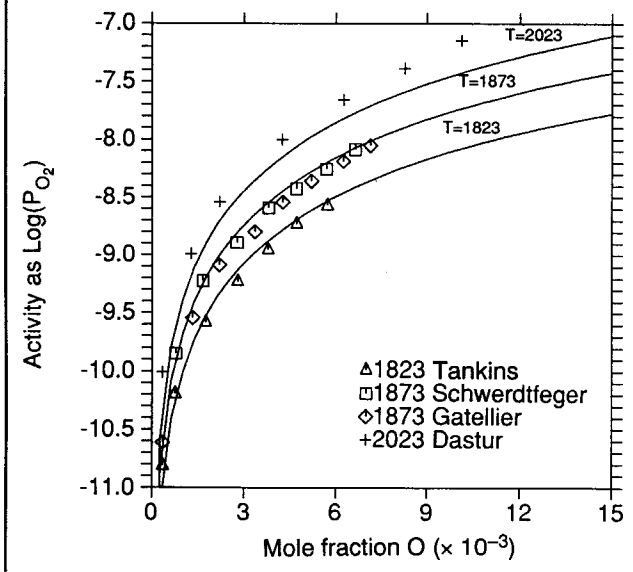

Fig. 12 Calculated vs experimental oxygen activity in Fe-O liquid.

and Fe^{+3} on the octahedral and tetrahedral sublattices. The final set of parameters, modified by a later overall optimization, are listed in Table 1, and the thermochemical properties of stoichiometric spinel are tabulated in Table 3. In Fig. 5, the heat capacity of spinel is plotted with experimental data, and in Fig. 6, the enthalpy is plotted. The heat capacity close to the magnetic transition is not described accurately due to limitations in the magnetic model, but the errors above and below the transition temperature compensate each other in the enthalpy description, where the agreement is very good.

The calculated oxygen potential inside the spinel is shown in Fig. 7. An enlargement around the stoichiometric composition is shown in Fig. 8. In Fig. 9, the degree of order is plotted for various temperatures. The agreement is very good.

Corundum

Corundum was described as a compound with fixed composition, and only the Gibbs energy of formation was evaluated using the available experimental data. The final set of parameters are given in Table 1, and in Table 4, the thermochemical properties of corundum are tabulated at various temperatures. In Fig. 10 and 11, the heat capacity and the enthalpy of corundum are plotted with experimental data. There is the same discrepancy in the description of the heat capacity data as for the spinel phase close

Table 5 Calculated Three-Phase Invariant Equilibria in the Fe-O System

Phases and compositions (X_O)	Temperature, K	Reference
bcc (2.1×10^{-7}), halite (0.5138), spinel (0.5713)	832	This work
	842	Barbi
	850	Barbi
	827	Barbero
fcc (6.8×10^{-6}), bcc (1.6×10^{-5}), halite (0.5120)	1185	Pure Fe
fcc (9.5×10^{-5}), liquid (0.5072), halite (0.5123)	1643	This work
	1644	Darken and Gurry
fcc (1.0×10^{-4}), bcc (2.1×10^{-4}), liquid (0.5069)	1664	Pure Fe
bcc (2.8×10^{-4}), liquid (4.95×10^{-3}), liquid (0.5055)	1802	This work
	1797	Darken and Gurry
Liquid (0.5419), wüstite (0.5451), spinel (0.5710)	1695	This work
	1697	Darken and Gurry
Spinel (0.5727), liquid (congruent transformation)	1870	This work
	1870	Darken and Gurry
Spinel (0.5736), liquid (0.5853), gas	1798	This work
	1856	Darken and Gurry
Spinel (0.5799), corundum (0.6), gas	1724	This work
	1730	Darken and Gurry

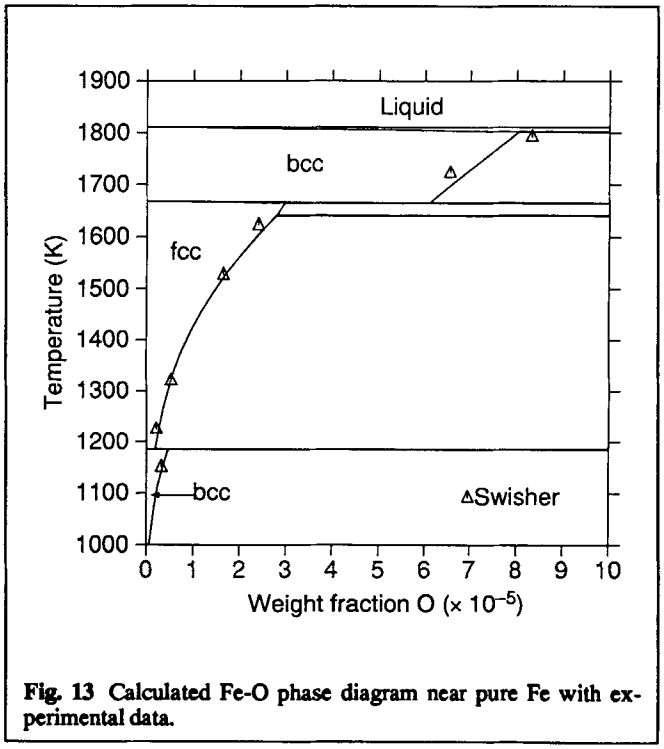

Fig. 13 Calculated Fe-O phase diagram near pure Fe with experimental data.

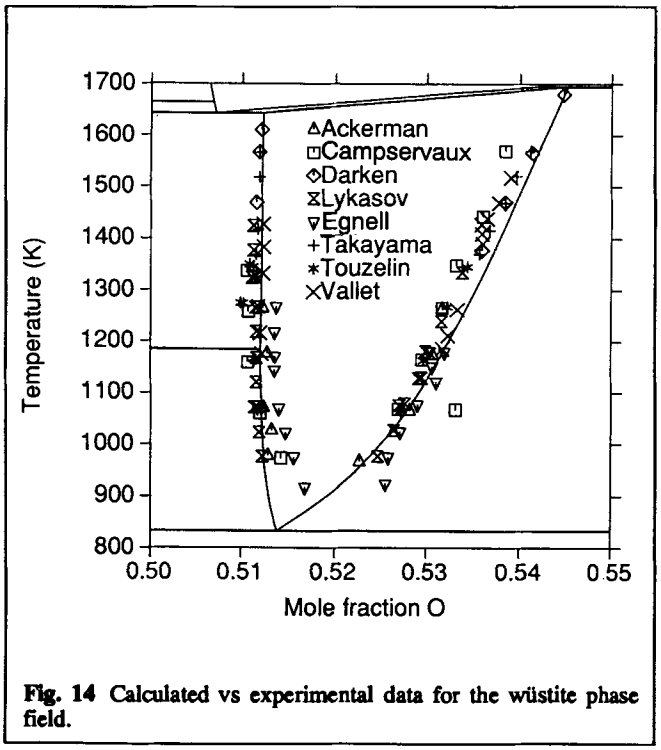

Fig. 14 Calculated vs experimental data for the wüstite phase field.

to the transition temperature. For the corundum, the lambda transition temperature, 943 K, was used, and a Bohr magneton number was evaluated as for spinel.

All Solid Compounds

When all solid oxides had been given a reasonable set of parameters, a second-step optimization was performed, varying all parameters at the same time and also including experimental information on invariant equilibria and measured activities in the two-phase regions. This resulted in a major adjustment of all parameters.

Liquid

The liquid phase was assessed after all solid oxides had been determined. In the first step, a reasonable agreement was obtained with the information in the binary system, using the select phase diagram data and thermochemical data. The parameter $G^0_{Fe^{+3}:Va}$ was set to a value of 200 000 J/mol higher than $G^0_{Fe^{+2}:Va}$ which represents real liquid iron, because there should be very little Fe^{+3} when there is no oxygen present. The actual value chosen had very little influence if it was sufficiently large.

An assessment of the Ca-Fe-O system made in parallel[48] indicated that the metastable extrapolation of the liquidus in equilibrium with fcc should be steeper than indicated by the very scarce experimental information in the binary system. Thus, a fictitious experimental point at 1473 K, obtained from extrapolation from experimental information on the liquid/fcc equilibria in the ternary system, was added. This forced the liquidus to become steeper and improved the agreement with experimental data in the ternary Ca-Fe-O system.

In Fig. 12, the calculated oxygen activities in the liquid at various temperatures close to pure Fe are shown with experimental data.

Total Optimization

A final run was made including all experimental data and varying all parameters in the system. This had very little effect on the total fit and the final set of parameters.

In Fig. 13, an enlargement of the phase diagram close to pure Fe is shown together with experimental data. Agreement is very good. In Fig. 14, the wüstite phase field is shown with experimental data from Ackerman and Sandford,[2] Darken and Gurry,[3] Takayama and Kimizuka,[15] Campservaux *et al.*,[49] Lykasov *et al.*,[50] Egnell,[51] Touzelin,[52] and Vallet and Raccah.[53] The calculated curve is well within the experimental scatter. The temperature for the lower three-phase equilibrium turned out to be 833 K, which is within the experimental uncertainty. The upper three-phase temperature with liquid and fcc was 1643 K, and the value reported by Darken and Gurry,[13] is 1644 K.

In Fig. 15, the complete Fe-O phase diagram is shown using weight percent vs temperature. All calculated three-phase equilibria are listed in Table 5 with experimental data. All values are within the assumed experimental uncertainties—the only significant deviation is for the three-phase equilibrium with spinel, liquid, and gas. Finally, in Fig. 16, the diagram is plotted again, but with oxygen potential instead of composition.

Final Remarks

The set of model parameters given in Table 1 is a consistent set of thermodynamic parameters that describes the iron-oxygen system. The advantage of having such a set is that it eases reliable extrapolations to higher temperatures or to higher order systems.

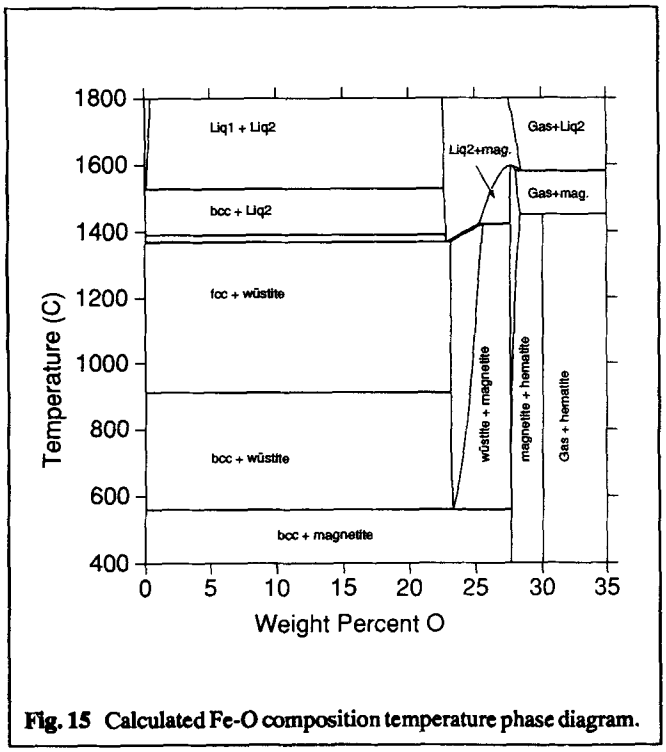

Fig. 15 Calculated Fe-O composition temperature phase diagram.

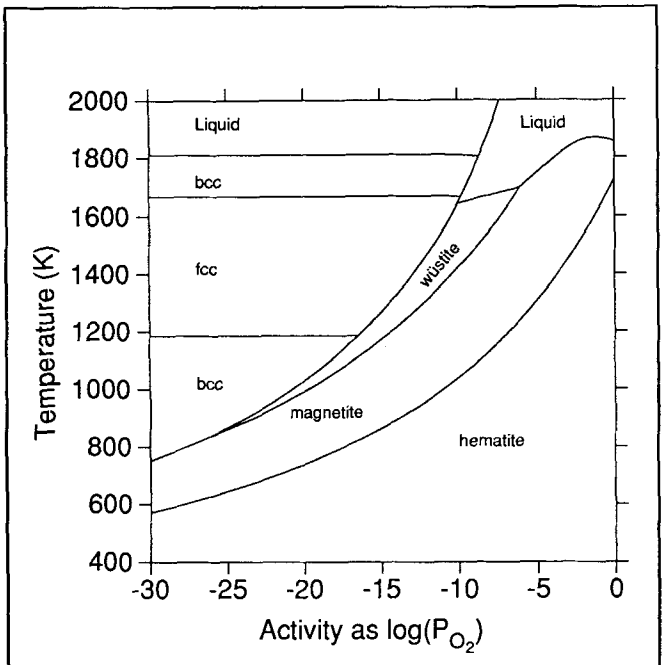

Fig. 16 Calculated Fe-O oxygen potential-temperature phase diagram.

The inclusion of ternary information in this binary assessment shows the importance of validating the assessment against data not only in the present system but also in higher order systems.

The author is greatly indebted to Professor Mats Hillert for advice and criticism during this work. Several valuable discussions with Dr. David Garvin of NIST Chemical Reference Data and Dr. John Haas at the National Geological Survey, Maryland, are also acknowledged, and also the contributions by Bo Jansson with the assessment of the magnetite phase. This work has been sponsored by a grant from STU, the Swedish Board for Technical Development, and NIF, Nordisk Industrifond.

Cited References

1. P.J. Spencer and O. Kubaschewski, *Calphad, 2,* 147-167 (1978).
2. R.J. Ackerman and R.W. Sandford, Jr., USAEC Rep. ANL 7250, Chemistry (TID-4500), Argonne, IL (1966).
3. L.S. Darken and R.W. Gurry, *J. Am. Chem. Soc., 67,* 1398-1412 (1945).
4. I. Bransky and A.Z. Hed, *J. Am. Ceram. Soc., 51,* 231-232 (1968).
5. F.E. Rizzo and J.V. Smith, *J. Phys. Chem., 72,* 485-488 (1968).
6. G.B. Barbi, *J. Phys. Chem., 68,* 2912-2916 (1964).
7. R.A. Giddings and R.S. Gordon, *J. Am. Ceram. Soc., 56,* 111-116 (1973).
8. R.L. Levin and J.B. Wagner, Jr., *Trans. Metall. Soc. AIME, 236,* 516-519 (1966).
9. B. Swaroop and J.B. Wagner, Jr., *Trans. Metall. Soc. AIME, 239,* 1215-1218 (1967).
10. F.E. Rizzo, R.S. Gordon, and I.B. Cutler, *J. Electrochem. Soc., 116,* 266-274 (1969).
11. M.F. Marion, *La Docum. Met.,* (24), 87-129 (1955).
12. J.R. Gavarri, C. Carel, and D. Weigel, *J. Solid State Phys., 29,* 81-95 (1979).
13. L.S. Darken and R.W. Gurry, *J. Am. Chem. Soc., 68,* 798-815 (1946).
14. O. Sjöden, S. Seetharaman, and L.-I. Staffansson, *Metall Trans. B, 17,* 179-184 (1986).
15. E. Takayama and N. Kimizuka, *J. Electrochem. Soc., 127,* 970-976 (1980).
16. C. Carel, *Compt. Rend. Hebd. C: Sci. Chim., 273,* 393-395 (1971).
17. J.A. Barbero, M.A. Blesa, and A.J.G. Maroto, *Z. Phys. Chem., 124,* 139-147 (1981).
18. S.S. Todd and K.R. Bonnickson, *J. Am. Chem. Soc., 73,* 3894-3895 (1951).
19. J.P. Coughlin, E.G. King, and K.R. Bonnickson, *J. Am. Chem. Soc., 73,* 3891-3893 (1951).
20. F. Grönvold and A. Sveen, *J. Chem. Thermodyn., 6,* 859-872 (1974).
21. W.A. Roth and W. Bertram, *Z. Electrochem. Angew. Phys. Chem., 35,* 297-308 (1929).
22. E.F. Westrum and F. Grönvold, *J. Chem. Thermodyn., 1,* 543-557 (1969).
23. H. Esser, R. Averdick, and W. Grass, *Arch. Eisenhüttenwes., 6,* 289-292 (1933).
24. G.B. Barbi, *J. Phys. Chem., 68,* 1025-1029 (1964).
25. R. Dieckmann, *Ber. Bunsenges. Phys. Chem., 86,* 112-118 (1982).
26. C.C. Wu and T.O. Mason, *J. Am. Ceram. Soc., 64,* 520-522 (1981).
27. E. Jacobson and E. Rosén, *Scand. J. Met., 10,* 39-43 (1981).
28. F.J. Norton, Rep. No. 55-RL-1248, General Electric Res. Lab. (1955).
29. F. Grönvold and E.J. Samuelsen, *J. Phys. Chem. Solids, 36,* 249-256 (1975).
30. K. Krupka, personal communication *via* J. Haas (1974).
31. F. Grönvold and E.F. Westrum, Jr., *J. Am. Chem. Soc., 81,* 1780-1783 (1959).
32. E.S. Tankins, N.A. Gokcen, and G.R. Belton, *Trans. Metall. Soc. AIME, 230,* 820 (1964).
33. K. Schwerdtfeger, *Trans. Metall. Soc. AIME, 239,* 1276-1281 (1967).
34. C. Gatellier and M. Olette, *Compt. Rend. C, 266,* 1133 (1968).
35. M.N. Dastur and J. Chipman, *Trans. Metall. Soc. AIME, 185,* 441 (1949).
36. M.T. Hepworth, R.P. Smith, and E.T. Turkdogan, *Trans. Metall. Soc. AIME, 236,* 1278-1283 (1966).
37. J.H. Swisher and E.T. Turkdogan, *Trans. Metall. Soc. AIME, 239,* 426-431 (1967).
38. I. Ansara and B. Sundman, SGTE, Proc. Conf. CODATA, Ottawa (1986).
39. T.I. Barry and F.P. Glasser, NPL Rep. DMA(A)169 (1988).
40. G. Inden, *Z. Metallkd., 66,* 577 (1975).
41. M. Hillert and M. Jarl, *Calphad, 2,* 227-238 (1978).
42. C.P. Chin, S. Hertzman, and B. Sundman, TRITA MAC 203 (1987).
43. A. Fernandez-Guillermet and P. Gustafson, *High Temp.—High Pressures, 16,* 591-610 (1985).
44. M. Hillert, B. Jansson, and B. Sundman, *Z. Metallkd., 79,* 81-87 (1988).
45. M. Hillert, B. Jansson, B. Sundman, and J. Ågren, *Metall Trans. A, 16,* 661-678 (1985).
46. B. Jansson, thesis, Royal Institute of Technology, Stockholm (1984).
47. B. Sundman, B. Jansson, and J.O. Andersson, *Calphad, 9,* 153-190 (1985).
48. M. Hillert, M. Selleby, and B. Sundman, *Metall. Trans. A, 21,* 2759-2766 (1990).
49. J. Campservaux, G. Boureau, C. Picard, and P. Gerdanian, *Ann. Chim., 5,* 250-260 (1970).
50. A.A. Lykasov, Yu.S. Kuznetsov, E.I. Pil'ko, V.I. Shishkov, and V.A. Kozheurov, *Russ. J. Phys. Chem., 43,* 1754 (1969).
51. H.-J. Egnell, *Arch. Eisenhüttenwes., 28,* 109-115 (1957).
52. B. Touzelin, *Rev. Int. Hautes Temp., 11,* 219-230 (1974).
53. P. Vallet and P. Raccah, *Mém. Sci. Rev. Métall., 62,* 1-29 (1965).